Biochimica et Biophysica Acta 1838 (2014) 3052–3060

Contents lists available at ScienceDirect

Biochimica et Biophysica Acta

journal homepage: www.elsevier.com/locate/bbamem

A new gating site in human aquaporin-4: Insights from molecular dynamics simulations

Domenico Alberga [a,c], Orazio Nicolotti [b,c], Gianluca Lattanzi [a,c], Grazia Paola Nicchia [d], Antonio Frigeri [d], Francesco Pisani [d], Valentina Benfenati [e], Giuseppe Felice Mangiatordi [b,*]

[a] Dipartimento Interateneo di Fisica "M. Merlin," Università di Bari "Aldo Moro," INFN, Via E. Orabona, 4, Bari I-70126, Italy
[b] Dipartimento di Farmacia, Scienze del Farmaco, Università di Bari "Aldo Moro," Via Orabona 4, Bari 70126, Italy
[c] Centro Ricerche TIRES, University of Bari "Aldo Moro," Via Amendola 173, Bari I-70126, Italy
[d] Department of Bioscience, Biotechnologies and Biopharmaceutics and Center of Excellence in Comparative Genomics, University of Bari "Aldo Moro," Bari 70126, Italy
[e] Consiglio Nazionale delle Ricerche (CNR), Istituto per la Sintesi Organica e la Fotoreattività (ISOF), Via Gobetti 101, Bologna 40129, Italy

ARTICLE INFO

Article history:
Received 9 May 2014
Received in revised form 23 July 2014
Accepted 12 August 2014
Available online 19 August 2014

Keywords:
Water transport
AQP4
Aquaporins
Molecular dynamics
Gating

ABSTRACT

Aquaporin-4 (AQP4) is the predominant water channel in different organs and tissues. An alteration of its physiological functioning is responsible for several disorders of water regulation and, thus, is considered an attractive target with a promising therapeutic and diagnostic potential. Molecular dynamics (MD) simulations performed on the AQP4 tetramer embedded in a bilayer of lipid molecules allowed us to analyze the role of spontaneous fluctuations occurring inside the pore. Following the approach by Hashido et al. [Hashido M, Kidera A, Ikeguchi M (2007) Biophys J 93: 373–385], our analysis on 200 ns trajectory discloses three domains inside the pore as key elements for water permeation. Herein, we describe the gating mechanism associated with the well-known selectivity filter on the extracellular side of the pore and the crucial regulation ensured by the NPA motifs (asparagine, proline, alanine). Notably, on the cytoplasmic side, we find a putative gate formed by two residues, namely, a cysteine belonging to the loop D (C178) and a histidine from loop B (H95). We observed that the spontaneous reorientation of the imidazole ring of H95 acts as a molecular switch enabling H-bond interaction with C178. The occurrence of such local interaction seems to be responsible for the narrowing of the pore and thus of a remarkable decrease in water flux rate. Our results are in agreement with recent experimental observations and may represent a promising starting point to pave the way for the discovery of chemical modulators of AQP4 water permeability.

1. Introduction

Water homeostasis is crucial for the physiology of all living cells. Depending on their lipid composition, all biological membranes have some intrinsic water permeability. However, in several tissues, water transport is strongly facilitated by the presence of protein channels called aquaporins, which mediate an osmotically driven bidirectional water flux [1].

Among the aquaporin family members, aquaporin-4 (AQP4) is the principal water channel in the central nervous system (CNS) [2–4] and is mainly expressed in areas in close contact with the cerebrospinal fluid or the blood vessels, as in cell plasma membranes of astrocytes [5]. From a structural point of view, it is characterized by six transmembrane helices forming a water-selective pore [6] (Fig. 1). Two different human isoforms of AQP4 have been identified, namely, M1 (32 kDa) and M23 (30 kDa). They share identical extracellular domain residues but M1 comprises 22 more amino acids at the cytoplasmic N terminus [7,8]. These isoforms are structured in the membrane as heterotetramers, with each monomer containing its own channel whose mechanism is independent from the others [9]. These tetramers may, in turn, aggregate to form supramolecular structures known as orthogonal arrays of particles (OAPs) [10–12].

It is now generally agreed that an alteration of AQP4 functionality plays a critical role in deafness [13,14] as well as in the formation of brain edema [15,16], nowadays considered the leading cause of mortality due to head trauma and stroke [16]. A well-controlled brain water homeostasis is, thus, of utmost importance for the stability of neuronal function, as recently pointed out by several studies [2,14,17,18]. Nevertheless, current treatments are limited to the administration of hyperosmolar agents as well as to neurosurgical decompression in order to extract brain water [19–21], while approaches based on molecules selectively biasing AQP4 functionality are still missing. Indeed, among the few molecules thus far identified as being able to interfere with AQP4 water permeability, most showed high toxicity and low selectivity [22–24]. In this context, an in-depth understanding of the

* Corresponding author. Tel.: +39 080 5442551; fax: +39 080 5442230.
E-mail address: giuseppe.mangiatordi@uniba.it (G.F. Mangiatordi).

http://dx.doi.org/10.1016/j.bbamem.2014.08.015
0005-2736/

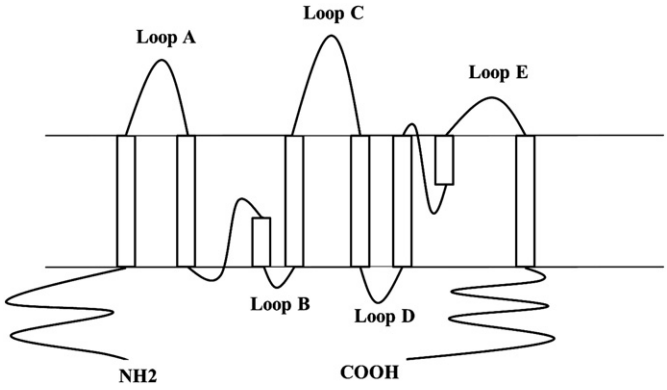

Fig. 1. 2D sketch of AQP4 structural elements.

water permeation mechanism in AQP4 is therefore strongly pursued in order to provide the basic knowledge for the development of rational approaches to drug design.

In this respect, the intense research efforts of the last years allowed to clarify, at the molecular level of detail, many issues related to the water flux mechanism in AQP4. It is commonly accepted that water permeability in AQP4, as well as in other aquaporins, is regulated by the presence of two oppositely oriented NPA motifs (asparagine, proline, and alanine; see Fig. 2) constituting a filter region in the middle of the channel [25–29]. Notably, because of its capacity to create a large electrostatic barrier, this region is able to contrast the proton permeation through the pore (proton exclusion mechanism) [28]. This selectivity is achieved by the formation of protein backbone collective macrodipoles. Together with the NPA region, the aromatic/arginine filter (ar/R) domain, also named selectivity filter (SF), which comprises residues H201 and R216 of AQP4, contributes to the proton permeation barrier [30] and is also critical to hindering the passage of other solutes mainly through a spatial restriction mechanism [31]. A complete free energy profile of the AQP4 channel was recently obtained by Cui and Bastien [32] on the basis of the Brownian dynamics fluctuation–dissipation theorem (BD-FDT) [33]. The emerged picture confirmed that, while the SF domain is responsible for water selectivity based on size constraints, the NPA motifs correspond to the maximum of the free-energy profile and hence regulate water permeation. Although this model is able to explain the water selectivity of the pore, some aspects, especially those related to water flux regulation, are still obscure. Indeed, experimental evidences suggest that eukaryotic aquaporins are frequently regulated post-translationally by gating mechanisms. Changes in divalent cation concentrations [34–36], in pH [34,35,37] and in osmolality [38,39] were proved to directly affect water permeability. Moreover, phosphorylation of conserved serine or threonine residues was also suggested to play a critical role in the gating of several aquaporins, including AQP4 [40,41]. Based on these assumptions, the water flux regulation might be causatively associated with the conformational change of a protein portion switching the opening/closure of the channel in response to a given external action. Importantly, Törnroth-Horsefield et al. provided new structural insights into eukaryotic aquaporin regulation through an in-depth analysis and comparison of the available X-ray structures [42]. According to this study, the water flux regulation could be related to the presence of a narrow constriction site at the cytoplasmic entry. Actually, the authors highlighted that this is clearly evident in different eukaryotic aquaporins such as SoPIP2;1, AQP0 and Aqy1. However, it was reported that the "water pore is undoubtedly open" at the cytoplasmic side in the crystal structure of human AQP4 (PDB code 3GD8 [6]). Beyond the mere analysis of the crystals, molecular dynamics (MD) simulations proved effective to obtain insights into the gating mechanism in aquaporins [43,44], as recently reported by Janosi and Ceccarelli [45], who showed a tap-like mechanism at the cytoplasmic end (CE) of AQP5 where the channel is closed by a translation of a histidine residue inside the pore. Such hypothesis relied not only on the analysis of the possible constriction effect of this local translation on the channel (analysis of the pore radius) but also on the calculation of the osmotic permeability (hereafter referred to as p_f; see references [46,47]) in the resulting different states (open and closed). In order to connect this scalar quantity to possible variations of the channel structure, the authors used a methodology proposed by Hashido et al. [47], which allows the description of contributions from local regions of a water channel to p_f based on MD simulations.

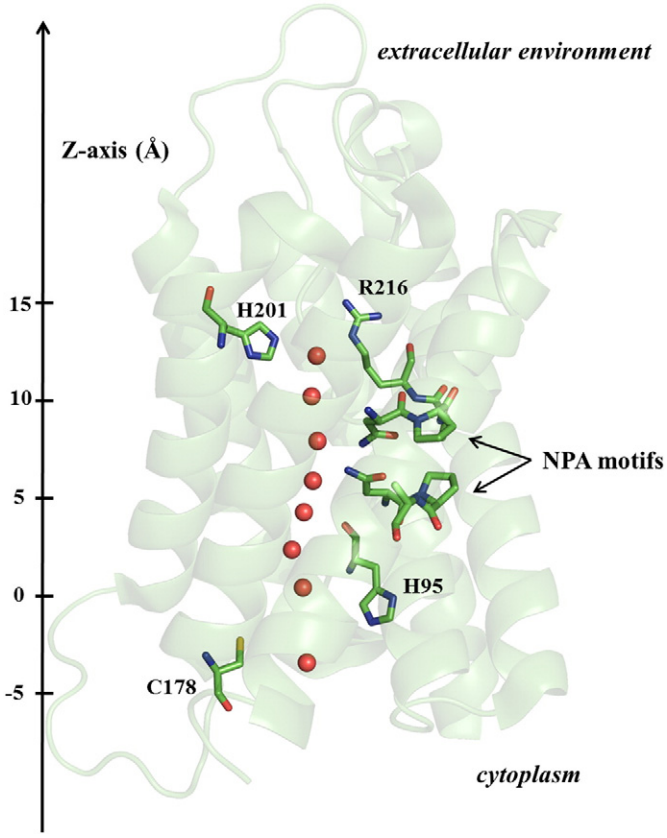

Fig. 2. X-ray solved structure of human AQP4 (PDB code 3GD8). Histidine at position 95 (H95), cysteine at position 178 (C178), important residues in the ar/R constricted selectivity filter (H201 and R216) and NPA motifs regions are rendered as sticks. Water molecules inside the pore are shown as spheres.

In the present study, we carried out MD simulations on the AQP4 tetramer and analyzed the obtained long trajectories following the same protocol used by Janosi and Ceccarelli [45]. We identified spontaneous fluctuations at the cytoplasmic end of the channel and assessed their influence on both water permeability rate and pore radius. The obtained results are supported by experimental evidences and allowed us to hypothesize a new gating mechanism for AQP4, hence providing valuable insights into the water regulation of this protein channel.

2. Results

All the results shown in the present section were obtained analyzing the calculated MD trajectory (195 ns at 310 K after 5 ns of equilibration). The MD simulations were carried out on the AQP4 tetramer embedded in a bilayer of lipid molecules (Fig. 3; see Materials and methods for simulation details). This section is organized as follows: first, we present the local osmotic permeability (p_{ii}) computed along the z-axis for all the monomers. Next, the time-dependent evolution of two representative distances and the local constriction indicators (LCIs) are discussed in order to identify the occurring local fluctuations inside the pore and their corresponding different states. Finally, selected representative

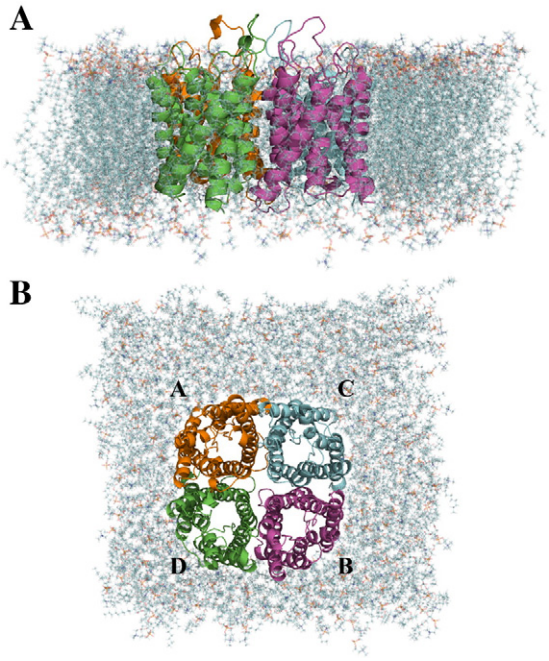

Fig. 3. Lateral (a) and top view with monomer labeling (b) of the simulated system. Water molecules are removed for simplicity. Each monomer of the tetramer is shown in a different color.

portions of simulations are analyzed taking into account the differences in terms of osmotic permeability and average pore radius.

2.1. Computation of the local osmotic permeability

The trajectory was subdivided in time intervals of 5 ns each, and the p_{ij} matrix was calculated for each monomer and each time interval. The z-axis was defined as the normal to the phospholipid bilayer with the origin in the position of the alpha carbon atom of residue A192 and pointing to the extracellular side. Fig. 4 shows the time evolution of the local osmotic permeability (diagonal elements of p_{ij} matrix) for each monomer along the z-axis of the channel. The four channels behave independently and offer a glimpse of the possible scenarios for water permeation in AQP4. Although the starting conformations of the channels are all open (characterized by the red color along the z-axis), a partial closure of the pore occurs at different times. This closure is located on the cytoplasmic side of the pore at negative values on the z-axis and is quite persistent in three out of four channels, as far as the time span of our simulations is concerned. A second, less persistent, event of water permeation impairment is triggered by a decrease of the permeation matrix element in a region that is close to the extracellular side and corresponds to the well-known selectivity filter. These results suggest the existence of a gating mechanism that is located at the bottom of the pore, close to the cytoplasmic end. This putative gating mechanism at the cytoplasmic end appears to be quite different from the selectivity filter on the extracellular side since it heavily affects the permeability of the pore.

2.2. Analysis of the local constriction indicators (LCIs)

Based on the obtained local osmotic permeabilities, we performed a closer inspection at the pore portions showing the major variations in terms of p_{ii}, namely, the SF domain (Z-coordinates ~ 12 Å) and the domain located at the cytoplasmic end, hereafter referred to as CE and corresponding to a Z-coordinate ~ −2 Å. The analysis of the trajectory shows that p_{ii} decreases when the pore is obstructed by the approach of R216 to H201 and/or H95 to C178. Based on this observation, we defined two local constriction indicators (LCIs): the first is $d_{SF,}$ which measures the distance between the nitrogen hydrogen bond (HB) acceptor atom of H201 and the closer terminal nitrogen atom of R216 at the selectivity filter (SF); the second is $d_{CE,}$ which measures the distance between the nitrogen HB acceptor atom of H95 and the sulfur atom of C178 at the CE (see Fig. 6). Noteworthy, the variation of d_{CE} is mainly due to the high mobility of the imidazole ring belonging to H95. Indeed, the RMSF computed for the H95 side chain is equal to 3.04 Å (vs. 1.20 for C178 side chain). On the contrary, no relevant motion of the main chain of H95 can be detected (RMSF = 1.70 Å).

The time dependence of the two LCIs is represented in Fig. 5. It is then evident that the two LCIs switch between two possible states. In particular, d_{SF} is close to 6 Å in the open conformation while its value is close to 3 Å in the closed conformation. As far as the selectivity filter is concerned, the closed conformation occurs at a low probability and, whenever it happens, the transition back to the open state is rather fast.

On the contrary, d_{CE} shows dramatic changes from an average value of 9 Å in the open conformation to an average value of 4 Å in the closed conformation. The transition to the closed conformation is more frequent (all the monomers display this transition within our total simulation time) and more persistent at least on the timescale of 200 ns. It is worth noting that in monomer D, permeation stops for a few nanoseconds although SF returns to the open state (Figs. 4 and 5). A possible explanation for this delay might be found in the occasional hindrance offered by loop C, which prevents the passage of water molecules for the time needed to reposition in the fully open conformation.

Building on this analysis, we decided to focus our attention on representative intervals of our trajectories (dotted lines in Fig. 5), corresponding to four possible situations characterized by the states (open/closed) of the SF and our putative second gate at the CE. In synthesis, analysis of the selected LCIs allowed us to identify not only the spontaneous fluctuations inside the pore affecting the osmotic water permeation but also the representative segments of trajectory for the possible different states of the water pore.

2.3. Analysis of representative segments of trajectory

The total osmotic permeabilities computed from the selected intervals of the trajectory are reported in Table 1. From the obtained p_f values, it is evident that the CE closure corresponds to a consistent drop of permeability to a value that is comparable to that obtained when the SF is closed. The permeability is further decreased when both gates are closed: it is questionable whether this “completely closed” state might have a physiological role for AQP4. However, the data in Table 1 suggest that there are three possible values for the osmotic permeabilities of AQP4 and confirm that the observed variations of p_f are directly related to variations of the selected LCIs.

For the same representative portions of the trajectory, we calculated the average pore radius as a function of the z-coordinate along the axis of the pore. The results are reported in Fig. 7a: it can be observed that there are four possible states, characterized by well-defined profiles of the protein pores. In particular, it is worth mentioning that the variation of the inner radius is quite small in the region of the selectivity filter, while it is by far more evident at the CE, where H95 effectively obstructs the pore. As shown in Fig. 7a, the pore radius profile of the open/open state nicely overlaps with that of the X-ray structure. Indirectly, this proves that the crystal structure represents an open/open state. In Fig. 7b, we report the obtained local osmotic permeabilities for the representative portions of the trajectory. These profiles bear a close resemblance to those of the pore radii in Fig. 7a. The role played by the second gate at the CE is confirmed by the effective drop in the osmotic permeability. Consistently, the NPA region acts as a filter, and its radius is not affected by the states of the two gates, while its osmotic permeability is directly correlated with the state of the selectivity filter on the extracellular side.

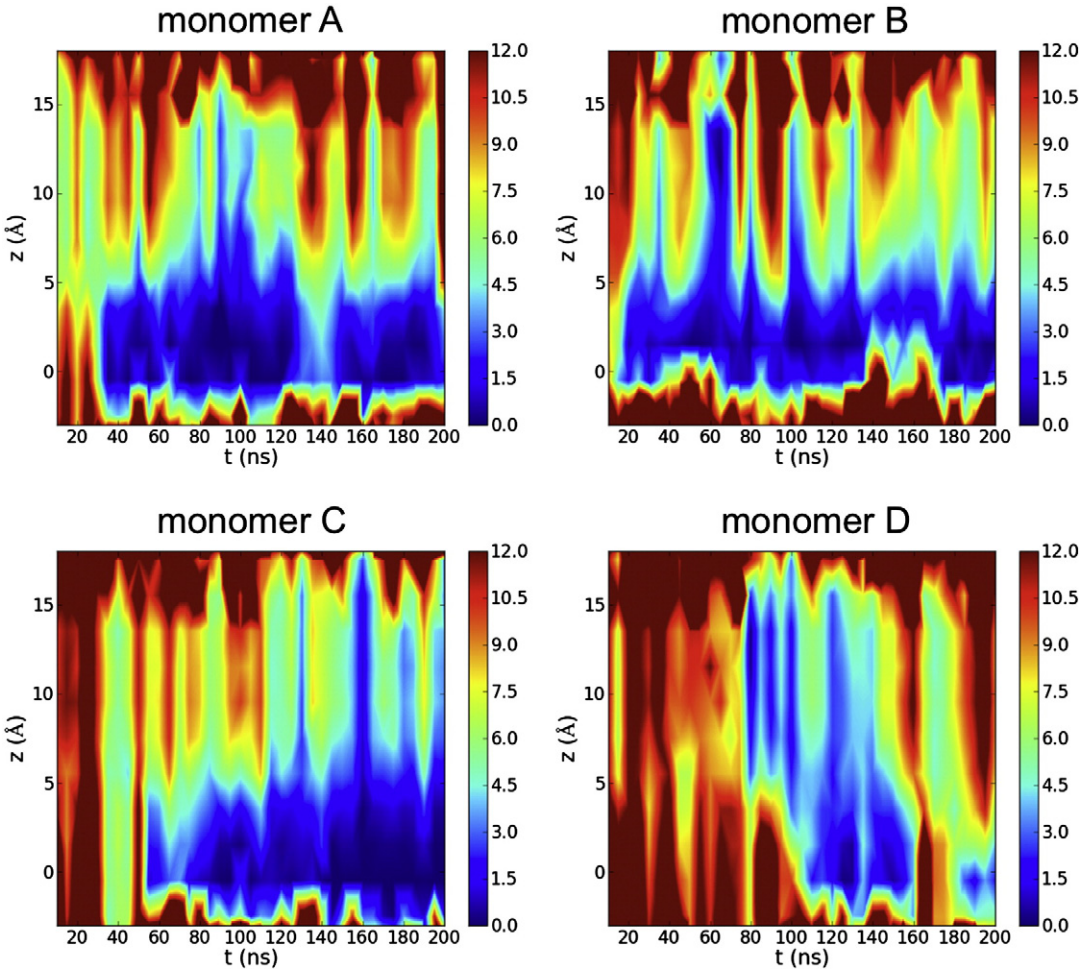

Fig. 4. Color plots showing the time-dependent evolution of the local osmotic permeability along the channel in the four monomers. The z (Å) values indicate the position inside the channel (see Fig. 2). Osmotic permeability values are expressed in units of 10^{-14} cm^3/s and were computed by subdividing the trajectories into 5-ns intervals. Note that such values refer to the local permeability sampled each 5 ns (for instance, $t = 10$ ns represents the local permeability computed in the range of 5 to 10 ns).

3. Discussion

Taken together, our results indicate the presence of four possible states of the AQP4 water pore depending on the fluctuation of single key residues, namely, R216 for the SF domain and H95 for the CE domain. Notably, the application of the approach developed by Zhu et al. [46] on intervals of MD trajectories, which are representative of these states, suggests that there are three possible values for the water permeabilities of AQP4 depending on the conformation of these key residues inside the pore: (1) high permeability (9.5×10^{-14} cm^3/s) when both states are in an open form; (2) low permeability (between 2.3 and 2.9×10^{-14} cm^3/s) after the closure of one of the states and (3) residual permeability (1.3×10^{-14} cm^3/s) if both states are in a closed form. It is worth noting that the obtained values are consistent with those obtained from experiments on membrane permeability (from 3.5 to 9×10^{-14} cm^3/s) in cells expressing AQP4 [48]. In this respect, the commonly accepted picture concerning the structure and dynamics of the AQP4 channel, based on the inspection of the crystal [42] as well as from the analysis of short MD simulations [32,47], should be critically revised. Indeed, our results indicate that the SF region may act not only as a selectivity filter (as already known) but also as a gating site depending on the fluctuation of R216, as already reported in recent MD simulations, but only after the application of large membrane potentials [49].

Even more interestingly, our data allow us to postulate the existence of a new crucial gating site, named CE, inside the pore characterized by the two residues H95 and C178 whose interaction is triggered by the rotation of the imidazole ring of H95. It is worth noting that, in the crystal structure, the nitrogen acceptor atom of the H95 side chain is engaged in hydrogen bonding with the oxygen atom of the T101 side chain, the main chain nitrogen atom of H95 interacts with the oxygen atom of the E41 side chain, and finally a water molecule bridges the sulfur atom of C178 and the nitrogen acceptor atom of the H95 side chain. Importantly, we observed that CE closure takes place after the reorientation of H95, whose new conformation implies the disruption of the interactions described above. In this regard, it is interesting to enquire why the closed conformation of that domain was not reported in the crystal structure: we speculate that the absence of a CE closed state in the crystal might be due to the experimental conditions likely favoring the occurrence of the open state because of low solvent entropic contributions at the experimental temperature of 77 K [6], or, for instance, the critical absence of the membrane bilayer that significantly alters the electrostatic framework.

This putative gating mechanism at the CE appears to be quite different from the SF on the extracellular side. Indeed, the time evolution of the considered LCIs suggest that, although it is possible to postulate a gating role for both SF and CE domains, variations at the level of the SF are less frequent and, when they occur, the closed state persists only for a few nanoseconds. In other words, the gating ability of the pore is mostly ascribable to the dynamics of H95 inside the channel. This is also supported by our analysis of the average pore radius: the reduction at the CE level is more pronounced than that of the SF domain whereas, in agreement with previous studies [25,47], no narrowing during the simulations is detected at the level of the NPA motifs, thus confirming the lack of any constriction effect at that level. To analyze the role of

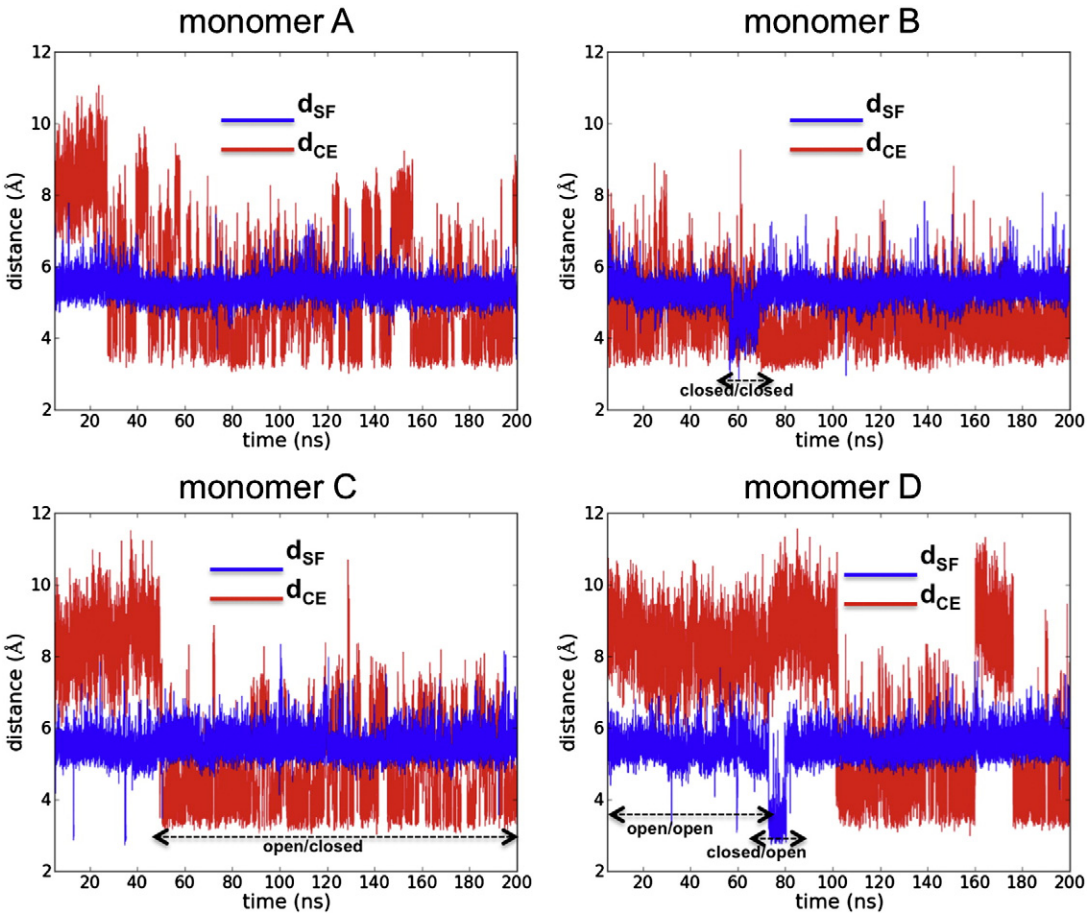

Fig. 5. Time dependent evolutions of the Local Constriction Indicators (LCIs) d_{SF} and d_{CE}. Representative segments of the trajectories are highlighted by a dotted line.

these key domains in water dynamics inside the pore, we extended our analysis of the representative sections of the trajectory by calculating the osmotic permeability correlation matrix in the four states. The results are reported in Fig. 8, where the extension of the red region indicates the amount of correlation between the movements of water molecules inside the channel: the ideal case of a chain of water molecules would correspond to a complete red square. This ordered transport of water molecules can be assigned approximately to the open/open case (top left side of Fig. 8). Concerning the NPA motifs, our correlation analysis confirms the indications by Hashido et al. [47]: the collective motion of the water chain is hindered by the NPA region, which divides the channel into two different sub-channels. Inside a single compartment, the motion of water molecules, whether adjacent or not, is strongly correlated. On the other hand, the correlation of the water molecules belonging to different sub-channels is moderate (off-diagonal elements of Fig. 8). This strict separation is evident by analyzing all four states and can be considered as the consequence of the water reorientation that is required to cross the NPA region. Furthermore, a

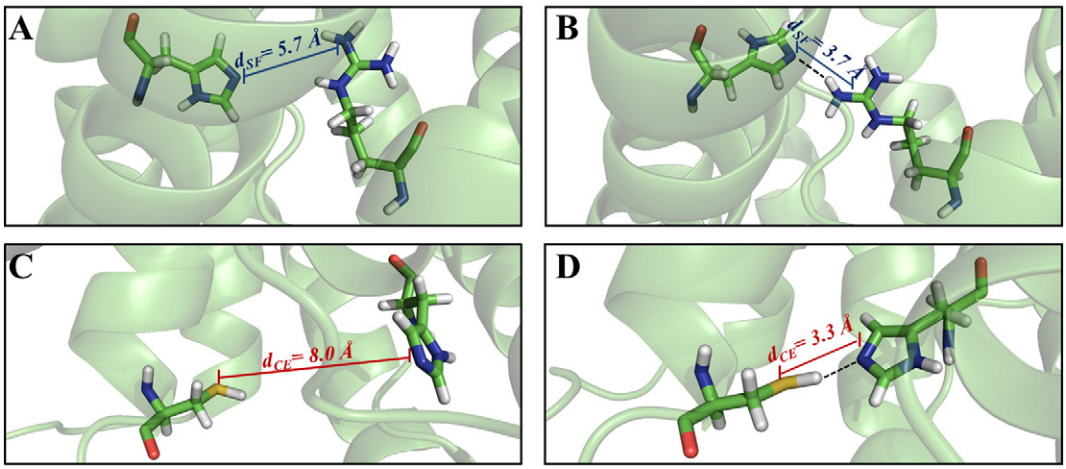

Fig. 6. Selected frames showing the different states (open and closed) of the SF and CE regions (lateral view). The zoomed monomers are depicted in cartoon representation while important residues in the ar/R constricted selectivity filter (SF) and cytoplasmic end (CE) are shown in sticks using the same colors as in Fig. 2. Local constriction indicators (LCIs) are shown by a continuous line while the H-bond interactions involving the residues in the closed states are depicted by a dotted line: A) SF open B) SF closed, C) CE open and D) CE closed.

Table 1
Osmotic permeabilities (p_f) of the representative segments of the trajectory corresponding to different states of the SF and CE regions. The value for the open/closed conformation is reported without standard deviation because it refers to a unique event.

Status (SF/CE)	p_f (10^{-14} cm^3/s)
Open/open	9.5 ± 2.1
Closed/open	2.9
Open/closed	2.3 ± 1.1
Closed/closed	1.3 ± 0.3

comparison of the four potential of mean force (PMF) profiles (obtained following the approach by Sasseville et al. [50]; see Supporting Information for methodological details) indicates that the energy barriers are closely related to the states of the two gates hypothesized in the present study (see Figure S3 in the Supporting Information).

It is important to remark that our study extends the time span of the trajectory analyzed by Hashido et al. (195 ns vs. 10 ns). In this respect, it is not surprising that the authors did not report any significant reduction in correlation around the ar/R region, contrary to what they expected. Indeed, as correctly postulated by Janosi and Ceccarelli [45], this was a rare event on the timescale of the MD trajectory by Hashido et al. [47]. Interestingly, our study reveals that the fluctuations of R216 may occasionally result in the closure of the SF domain on a typical timescale of a few nanoseconds, thus reducing the total osmotic permeability. Moreover, our analysis suggests that the SF can act as a critical gate only when the state of the CE gate is open (see Fig. 7b). Hence, the rate-limiting region for AQP4 should actually be located at the CE of the pore, differently from what has been previously postulated.

Building on these findings, it is certainly easy to postulate that the relative stability of the two resulting states (open and closed) may also depend on small changes (possible external stimuli) in the microenvironment, as already postulated for other AQPs. Notably, it was already proved that even small variations of pH can affect aquaporins and their functioning. For instance, all plant aquaporins are gated by a change in cytoplasmic pH [51]. In SoPIP2;1 (spinach plasma membrane aquaporin) the pH-dependent protonation state of a histidine regulates gating [52]. Importantly, this histidine in SoPIP2;1 belongs to an intracellular loop, exactly as in the case of H95 in AQP4. Leitao et al. [52] reported pH regulation of another plant aquaporin, namely, TIP2;1 (*Vitis vinifera*) showing that water permeability strongly decreases after a change in cytosolic pH. Again, a histidine belonging to a cytoplasmic loop (H131) was proved to be responsible for such pH sensitivity, which is lost upon mutation to alanine or aspartic acid.

Finally, it is worth noting that the proposed gating mechanism at the CE not only has some analogies with the mechanisms proposed for other aquaporins [42,44] but, concerning AQP4 itself, it is also consistent with some experimental evidences. Mutagenesis analysis performed by Yukutake et al. [53,54] revealed that divalent cations such as copper (Cu^{2+}), mercury (Hg^{2+}) and zinc (Zn^{2+}) inhibit AQP4 permeability by interacting with the sole C178, a key residue of the CE domain. Anyway, there is large agreement that proteins coordinate divalent cations by residues, which are, with few exceptions, cysteines, histidines and glutamates/aspartates. However, Yukutake et al. [53], inspecting the X-ray human AQP4 solved structure, reported that the simultaneous interactions of bivalent cations with C178 and other potentially involved residues are difficult to hypothesize. From our MD findings, we can instead postulate that divalent cations could significantly reduce water permeability by interacting simultaneously with C178 and H95, hence promoting the closure of the CE domain. MD simulations performed on two different mutants (H95G and C178S) also support the great relevance of such residues in CE gating. Indeed, the analysis of the obtained trajectories (40 ns for each mutant) indicates that upon replacement of H95 with glycine, the CE closure is not observed in any of the four monomers, thus confirming the key role in the proposed gating mechanism of the histidine. This is clearly shown in Figure S1 (see Supporting Information) where the time evolutions of the local constriction indicators (LCIs) are reported. For the WT, 40 ns of simulations were enough to observe the CE closure in two of the four monomers (see Fig. 5), while the four independent monomers in H95G display only the open state for the CE gate. This is even more evident when we compute the osmotic permeability (p_f): the obtained value (averaged over the four monomers) is equal to $9.6 \pm 2.8 \times 10^{-14}$ cm^3/s, fully comparable to that obtained for the open/open state of WT ($9.5 \pm 2.1 \times 10^{-14}$ cm^3/s).

On the contrary, the replacement of a C178 with another H-bond donor (S178) triggers the CE closure in three out of four monomers within 40 ns of MD simulations, as shown in Figure S2 (Supporting Information). This supports our hypothesis that an H-bond interaction is responsible for the narrowing of the pore and of the consequent remarkable decrease in water flux rate. Such interaction is formed by the H-bond donor residue at position 178 (cysteine or serine) and H95 playing as H-bond acceptor. Indeed, H-bond interactions between serine (donor) and histidine (acceptor) are already known in the literature (see for instance the charge relay network of serine proteases [55]), although the replacement of a thiol group ($pK_a \approx 8.3$) with a hydroxyl group ($pK_a \approx 13$) weakens the H-bond donor capacity.

In conclusion, the obtained data allowed us (i) to confirm the crucial role of the NPA motifs in water reorientation; (ii) to investigate the

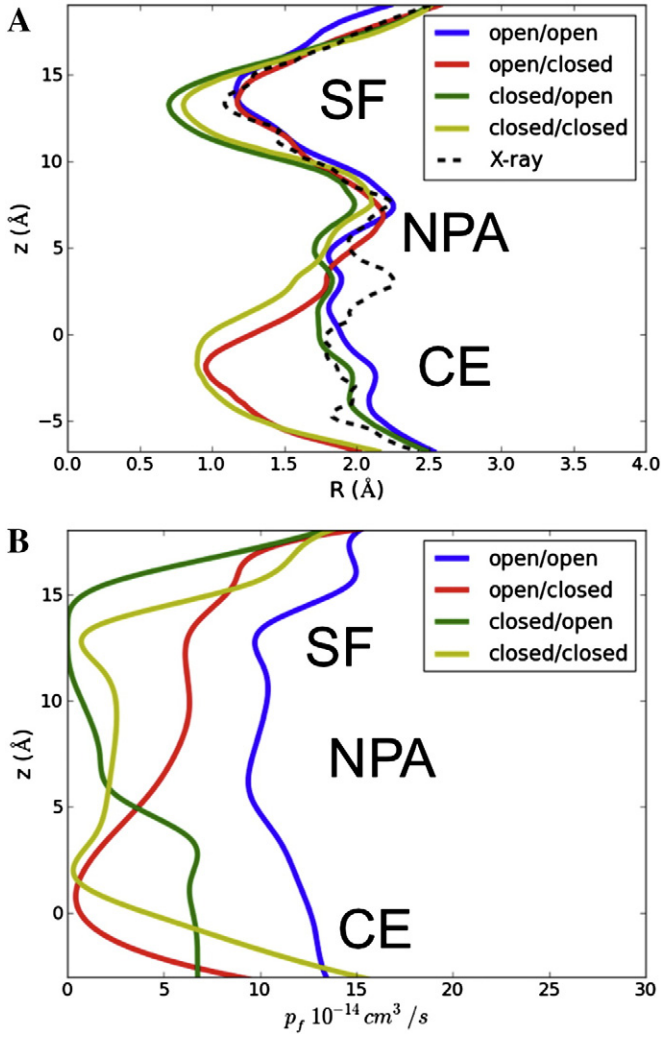

Fig. 7. Pore radius and local permeation among the different states. (a) Comparison of the five pore radius R(Å) profiles along the z-axis obtained for the considered states and the X-ray structure. All values are expressed in angstroms and the profiles of the four states are obtained by averaging the representative segments of simulations. (b) Calculated local permeation in the four representative segments of the simulations. The obtained data points were fitted by cubic splines.

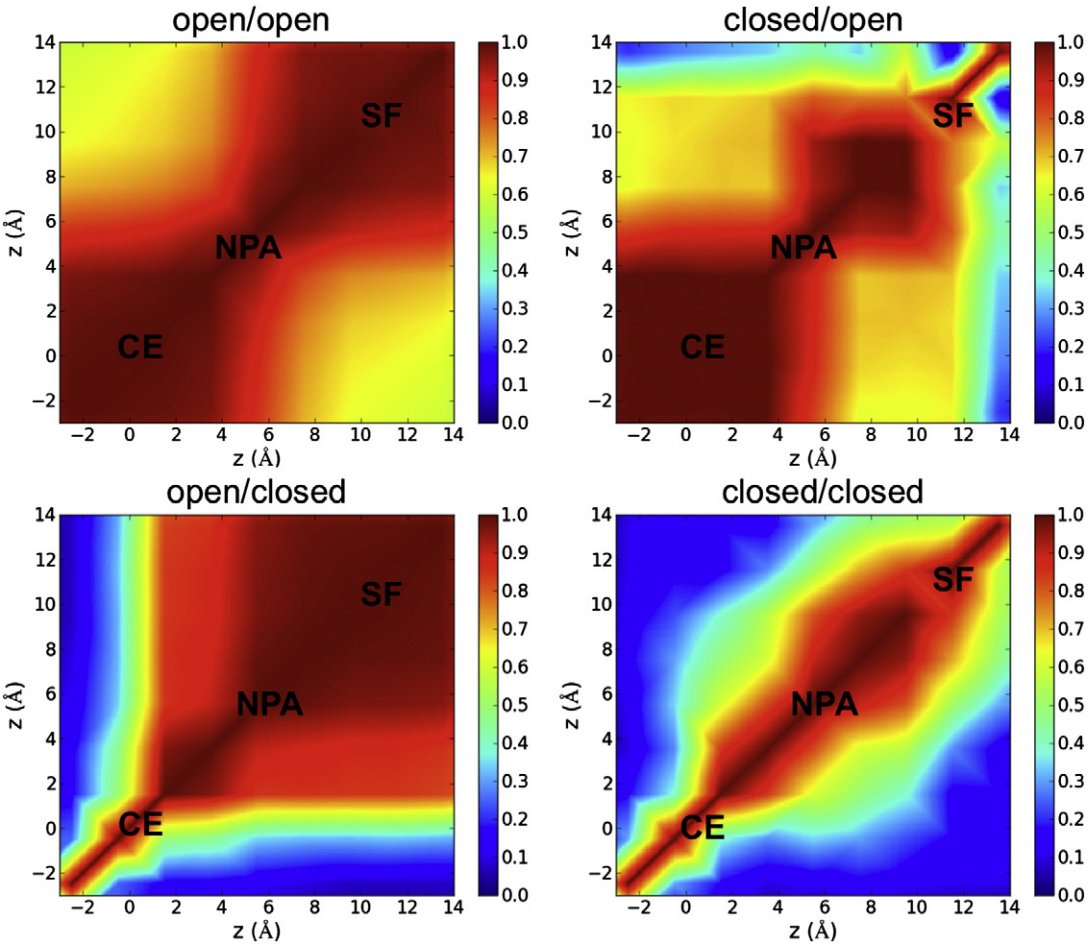

Fig. 8. c_{ij} correlation matrices obtained over the representative segments of simulations. Each state is indicated following the scheme SF/CE (see Table 1).

function of the SF which, besides the well-known role for water selection, appears characterized by a moderate ability of gating and (iii) to hypothesize the presence of a new crucial domain inside the pore at the CE of the water channel. Our data suggest that the spontaneous fluctuation of H95 inside the pore depends on the chance of establishing an H-bond interaction with C178 whose occurrence can strongly decrease osmotic water permeability. From a broader point of view, we do believe that this work represents a valuable contribution to the state of the art: thus far, "MD simulations of AQP4 have not revealed any blocking residue that may get extended into the pore and restrict the passage of water," as pointed out by a very recent review by Sachdeva and Singh [56]. The importance of this fluctuation, the stability of the resulting states (open and closed) and the associated changes in osmotic water permeation, all put forward this domain as a relevant gating site in AQP4. This hypothesis provides valuable insights into the AQP4 pore structure and dynamics and represents a promising starting point for the rational design of new modulators.

4. Methods

4.1. From X-ray structure to model system preparation

The initial structure of AQP4 was obtained from the Protein Data Bank (PDB), entry 3GD8 [6]. The obtained crystal was first pretreated using MAESTRO protein preparation module (version 9.5 [57]), which enables us to add missing hydrogen atoms and to determine the optimal protonation states for histidine residues. The simulation system was built as follows: a 120 × 120 $Å^2$ POPC (1-palmitoyl,2-oleoyl-sn-glycero-3-phosphocholine) bilayer patch was first built using the membrane plug-in of VMD (visual molecular dynamics) [58], with the membrane normal along the *z*-axis. A tetramer of AQP4 was embedded in this bilayer and lipid molecules within 0.8 Å of heavy atoms of the protein were removed. All protein atoms and crystallographic water molecules were kept fixed allowing only lipid molecules to equilibrate in vacuum for 200 ps. The obtained system was inserted into a periodic box extended by 18 Å in each direction from all protein atoms and filled with TIP3P water molecules [59], using the "solvate" plug-in of VMD. Twenty-three Na^+ and 19 Cl^- ions were added using VMD's autoionize plug-in, generating a 100 mM ionic concentration and a final electrically neutral system of 135,833 atoms. This system was again equilibrated with protein atoms and crystallographic water molecules at fixed positions for another 200 ps. The obtained system was finally relaxed for 200 ps, applying harmonic restraints only to the protein atoms (force constant of 1 kcal/mol/$Å^2$).

4.2. Molecular dynamics simulations

All MD simulations were performed using NAMD 2.9 [60] and the CHARMM27 force field [61]. The full system was minimized to remove steric clashes in the initial geometry and gradually heated up to 310 K within 500 ps of MD. The SHAKE algorithm was employed to constrain all R–H bonds. Periodic boundary conditions were applied in all directions. A non-bonded cutoff of 12 Å was used, whereas the particle mesh Ewald (PME) [62] was employed to include the contributions of long-range interactions. All simulations were performed in an isothermal-isobaric ensemble (1 atm, 310 K) with a Nosè–Hoover Langevin barostat [63,64] (oscillation period 200 fs, decay coefficient 100 fs) and a Langevin thermostat [65] (damping coefficient 1 ps^{-1}). The time step was set to

2 fs, and coordinates were saved every 1000 steps (2 ps). MD trajectories of 200 ns (for wild type) and of 40 ns (for each of the mutated proteins, C178S and H95G) were obtained. For all the considered systems, the equilibration of the structure required less than 5 ns and thus the first 5 ns were removed from the analysis. All simulations were performed on the FERMI supercomputer at CINECA, Italy.

4.3. Calculation of the osmotic permeability

The osmotic permeability matrix was calculated in the framework of the theory proposed by Zhu et al. [46]. The first step consisted in the computation of the variable *dn*:

$$dn = \sum_{i \in S(t)} dz_i / L$$

where dz_i is the displacement of the water molecule i along the z direction within the time interval dt and $S(t)$ is the set of water molecules inside the channel of length L at time t.

If $n(t)$ is the integral of dn over time, the total diffusion coefficient D_n is given by the mean square displacement as follows:

$$\left\langle n^2(t) \right\rangle = 2D_n t + C$$

Finally, the osmotic permeability was computed as:

$$p_f = v_W D_n$$

where v_W is the average volume occupied by a single water molecule.

This approach was used by Janosi and Ceccarelli [45] to describe water permeability in AQP5 and returns a single value of permeability for the whole channel. However, it does not provide any information related to the local structure of the channel (i.e. bottlenecks). In this work, we used the approach developed by Hashido et al. [47], which yields different values of permeability for each channel zone. To this aim, we subdivided the water channel in N sectors of length $L_N = 2$ Å and calculated the matrix $p_{ij} = v_W D_{ij}$ where $\langle n_i(t) n_j(t) \rangle = 2D_{ij}t + C$ and i and j are the indexes related to the i-th and j-th channel zones, respectively. The diagonal elements of the matrix p_{ii} represent the local permeability in the i-th zone, while the off diagonal elements express the covariance between the water molecules in the i-th zone and those in the j-th zone. The correlation matrix $c_{ij} = p_{ij}/(p_{ii}p_{jj})^{1/2}$ is a useful quantity that can be directly calculated from the permeability matrix p_{ij}.

Finally, the total permeation in the whole channel is recovered by the formula:

$$p_f = \sum_{i,j} p_{ij} / N^2$$

4.4. Computation of the average pore radius

The pore radius profile was calculated using the approach developed by Smart et al. [66]. Starting from a guess position and using a Monte Carlo procedure, it allows the calculation of the minimum pore radius for each coordinate value on the z-axis.

Acknowledgments

We acknowledge the CINECA awards nos. HP10CL5BLB-hAQP4 and HP10B4VZO7-epi-NMO under the ISCRA initiative for the availability of high-performance computing resources and support. This work was funded under the program FIRB (Futuro in Ricerca 2012, RBFR12SJA8_003).

Appendix A. Supplementary data

Supplementary data to this article can be found online at http://dx.doi.org/10.1016/j.bbamem.2014.08.015.

References

[1] M. Borgnia, S. Nielsen, A. Engel, P. Agre, Cellular and molecular biology of the aquaporin water channels, Annu. Rev. Biochem. 68 (1999) 425–458, http://dx.doi.org/10.1146/annurev.biochem.68.1.425.
[2] M. Amiry-Moghaddam, O.P. Ottersen, The molecular basis of water transport in the brain, Nat. Rev. Neurosci. 4 (2003) 991–1001, http://dx.doi.org/10.1038/nrn1252.
[3] S. Nielsen, E.A. Nagelhus, M. Amiry-Moghaddam, C. Bourque, P. Agre, et al., Specialized membrane domains for water transport in glial cells: high-resolution immunogold cytochemistry of aquaporin-4 in rat brain, J. Neurosci. 17 (1997) 171–180.
[4] A. Frigeri, M.A. Gropper, F. Umenishi, M. Kawashima, D. Brown, et al., Localization of MIWC and GLIP water channel homologs in neuromuscular, epithelial and glandular tissues, J. Cell Sci. 108 (Pt 9) (1995) 2993–3002.
[5] K. Yoneda, N. Yamamoto, K. Asai, K. Sobue, Y. Fujita, et al., Regulation of aquaporin-4 expression in astrocytes, Mol. Brain Res. 89 (2001) 94–102, http://dx.doi.org/10.1016/S0169-328X(01)00067-5.
[6] J.D. Ho, R. Yeh, A. Sandstrom, I. Chorny, W.E.C. Harries, et al., Crystal structure of human aquaporin 4 at 1.8 Å and its mechanism of conductance, Proc. Natl. Acad. Sci. 106 (2009) 7437–7442, http://dx.doi.org/10.1073/pnas.0902725106.
[7] F. Umenishi, A.S. Verkman, Isolation and functional analysis of alternative promoters in the human aquaporin-4 water channel gene, Genomics 50 (1998) 373–377, http://dx.doi.org/10.1006/geno.1998.5337.
[8] B. Yang, T. Ma, A.S. Verkman, cDNA cloning, gene organization, and chromosomal localization of a human mercurial insensitive water channel. Evidence for distinct transcriptional units, J. Biol. Chem. 270 (1995) 22907–22913, http://dx.doi.org/10.1074/jbc.270.39.22907.
[9] J.D. Neely, B.M. Christensen, S. Nielsen, P. Agre, Heterotetrameric composition of aquaporin-4 water channels, Biochemistry (Mosc) 38 (1999) 11156–11163, http://dx.doi.org/10.1021/bi990941s.
[10] M. Tajima, J.M. Crane, A.S. Verkman, Aquaporin-4 (AQP4) associations and array dynamics probed by photobleaching and single-molecule analysis of green fluorescent protein-AQP4 chimeras, J. Biol. Chem. 285 (2010) 8163–8170, http://dx.doi.org/10.1074/jbc.M109.093948.
[11] B.-J. Jin, A. Rossi, A.S. Verkman, Model of aquaporin-4 supramolecular assembly in orthogonal arrays based on heterotetrameric association of M1-M23 isoforms, Biophys. J. 100 (2011) 2936–2945, http://dx.doi.org/10.1016/j.bpj.2011.05.012.
[12] G.P. Nicchia, M. Mastrototaro, A. Rossi, F. Pisani, C. Tortorella, et al., Aquaporin-4 orthogonal arrays of particles are the target for neuromyelitis optica autoantibodies, Glia 57 (2009) 1363–1373, http://dx.doi.org/10.1002/glia.20855.
[13] G.P. Nicchia, R. Ficarella, A. Rossi, I. Giangreco, O. Nicolotti, et al., D184E mutation in aquaporin-4 gene impairs water permeability and links to deafness, Neuroscience 197 (2011) 80–88, http://dx.doi.org/10.1016/j.neuroscience.2011.09.023.
[14] J. Li, A.S. Verkman, Impaired hearing in mice lacking aquaporin-4 water channels, J. Biol. Chem. 276 (2001) 31233–31237, http://dx.doi.org/10.1074/jbc.M104368200.
[15] Z. Zador, S. Stiver, V. Wang, G.T. Manley, Role of aquaporin-4 in cerebral edema and stroke, Handb. Exp. Pharmacol. 159–170 (2009), http://dx.doi.org/10.1007/978-3-540-79885-9_7.
[16] M.C. Papadopoulos, A.S. Verkman, Aquaporin-4 and brain edema, Pediatr. Nephrol. Berl. Ger. 22 (2007) 778–784, http://dx.doi.org/10.1007/s00467-006-0411-0.
[17] D.K. Binder, X. Yao, Z. Zador, T.J. Sick, A.S. Verkman, et al., Increased seizure duration and slowed potassium kinetics in mice lacking aquaporin-4 water channels, Glia 53 (2006) 631–636, http://dx.doi.org/10.1002/glia.20318.
[18] M. Simard, M. Nedergaard, The neurobiology of glia in the context of water and ion homeostasis, Neuroscience 129 (2004) 877–896, http://dx.doi.org/10.1016/j.neuroscience.2004.09.053.
[19] A.T. Ogden, S.A. Mayer, E.S. Connolly Jr., Hyperosmolar agents in neurosurgical practice: the evolving role of hypertonic saline, Neurosurgery 57 (2005) 207–215.
[20] D. Palestrant, J.A. Frontera, S.A. Mayer, Treatment of massive cerebral infarction, Curr. Neurol. Neurosci. Rep. 5 (2005) 494–502.
[21] S. Subramaniam, M.D. Hill, Massive cerebral infarction, Neurologist 11 (2005) 150–160, http://dx.doi.org/10.1097/01.nrl.0000159987.70461.d7.
[22] J. Kato, M.K. Hayashi, S. Aizu, Y. Yukutake, J. Takeda, et al., A general anaesthetic propofol inhibits aquaporin-4 in the presence of Zn^{2+}, Biochem. J. 454 (2013) 275–282, http://dx.doi.org/10.1042/BJ20130046.
[23] A.J. Yool, E.A. Brown, G.A. Flynn, Roles for novel pharmacological blockers of aquaporins in the treatment of brain oedema and cancer, Clin. Exp. Pharmacol. Physiol. 37 (2010) 403–409, http://dx.doi.org/10.1111/j.1440-1681.2009.05244.x.
[24] V.J. Huber, M. Tsujita, T. Nakada, Identification of aquaporin 4 inhibitors using in vitro and in silico methods, Bioorg. Med. Chem. 17 (2009) 411–417, http://dx.doi.org/10.1016/j.bmc.2007.12.040.
[25] B. Ilan, E. Tajkhorshid, K. Schulten, G.A. Voth, The mechanism of proton exclusion in aquaporin channels, Proteins 55 (2004) 223–228, http://dx.doi.org/10.1002/prot.20038.
[26] B.L. De Groot, H. Grubmüller, The dynamics and energetics of water permeation and proton exclusion in aquaporins, Curr. Opin. Struct. Biol. 15 (2005) 176–183, http://dx.doi.org/10.1016/j.sbi.2005.02.003.

[27] H. Sui, B.G. Han, J.K. Lee, P. Walian, B.K. Jap, Structural basis of water-specific transport through the AQP1 water channel, Nature 414 (2001) 872–878, http://dx.doi.org/10.1038/414872a.
[28] M. Jensen, E. Tajkhorshid, K. Schulten, Electrostatic tuning of permeation and selectivity in aquaporin water channels, Biophys. J. 85 (2003) 2884–2899.
[29] N. Chakrabarti, E. Tajkhorshid, B. Roux, R. Pomès, Molecular basis of proton blockage in aquaporins, Structure 12 (2004) 65–74, http://dx.doi.org/10.1016/j.str.2003.11.017.
[30] H. Li, H. Chen, C. Steinbronn, B. Wu, E. Beitz, et al., Enhancement of proton conductance by mutations of the selectivity filter of aquaporin-1, J. Mol. Biol. 407 (2011) 607–620, http://dx.doi.org/10.1016/j.jmb.2011.01.036.
[31] J.S. Hub, B.L. de Groot, Mechanism of selectivity in aquaporins and aquaglyceroporins, Proc. Natl. Acad. Sci. 105 (2008) 1198–1203, http://dx.doi.org/10.1073/pnas.0707662104.
[32] Y. Cui, D.A. Bastien, Water transport in human aquaporin-4: molecular dynamics (MD) simulations, Biochem. Biophys. Res. Commun. 412 (2011) 654–659, http://dx.doi.org/10.1016/j.bbrc.2011.08.019.
[33] L.Y. Chen, D.A. Bastien, H.E. Espejel, Determination of equilibrium free energy from nonequilibrium work measurements, Phys. Chem. Chem. Phys. 12 (2010) 6579–6582, http://dx.doi.org/10.1039/B926889H.
[34] K.L. Németh-Cahalan, K. Kalman, J.E. Hall, Molecular basis of pH and Ca2+ regulation of aquaporin water permeability, J. Gen. Physiol. 123 (2004) 573–580, http://dx.doi.org/10.1085/jgp.200308990.
[35] M. Zelenina, A.A. Bondar, S. Zelenin, A. Aperia, Nickel and extracellular acidification inhibit the water permeability of human aquaporin-3 in lung epithelial cells, J. Biol. Chem. 278 (2003) 30037–30043, http://dx.doi.org/10.1074/jbc.M302206200.
[36] M. Zelenina, S. Tritto, A.A. Bondar, S. Zelenin, A. Aperia, Copper inhibits the water and glycerol permeability of aquaporin-3, J. Biol. Chem. 279 (2004) 51939–51943, http://dx.doi.org/10.1074/jbc.M407645200.
[37] C. Tournaire-Roux, M. Sutka, H. Javot, E. Gout, P. Gerbeau, et al., Cytosolic pH regulates root water transport during anoxic stress through gating of aquaporins, Nature 425 (2003) 393–397, http://dx.doi.org/10.1038/nature01853.
[38] M.J. Tamás, S. Karlgren, R.M. Bill, K. Hedfalk, L. Allegri, et al., A short regulatory domain restricts glycerol transport through yeast Fps1p, J. Biol. Chem. 278 (2003) 6337–6345, http://dx.doi.org/10.1074/jbc.M209792200.
[39] I. Johansson, C. Larsson, B. Ek, P. Kjellbom, The major integral proteins of spinach leaf plasma membranes are putative aquaporins and are phosphorylated in response to Ca2+ and apoplastic water potential, Plant Cell 8 (1996) 1181–1191.
[40] M. Zelenina, S. Zelenin, A.A. Bondar, H. Brismar, A. Aperia, Water permeability of aquaporin-4 is decreased by protein kinase C and dopamine, Am. J. Physiol. Renal Physiol. 283 (2002) F309–F318, http://dx.doi.org/10.1152/ajprenal.00260.2001.
[41] E. Gunnarson, M. Zelenina, G. Axehult, Y. Song, A. Bondar, et al., Identification of a molecular target for glutamate regulation of astrocyte water permeability, Glia 56 (2008) 587–596, http://dx.doi.org/10.1002/glia.20627.
[42] S. Törnroth-Horsefield, K. Hedfalk, G. Fischer, K. Lindkvist-Petersson, R. Neutze, Structural insights into eukaryotic aquaporin regulation, FEBS Lett. 584 (2010) 2580–2588, http://dx.doi.org/10.1016/j.febslet.2010.04.037.
[43] J.A. Garate, N.J. English, J.M. MacElroy, Human aquaporin 4 gating dynamics in dc and ac electric fields: a molecular dynamics study, J. Chem. Phys. 134 (2011) 055110, http://dx.doi.org/10.1063/1.3529428.
[44] E. Yamamoto, T. Akimoto, Y. Hirano, M. Yasui, K. Yasuoka, 1/f fluctuations of amino acids regulate water transportation in aquaporin 1, Phys. Rev. E. 89 (2014) 022718, http://dx.doi.org/10.1103/PhysRevE.89.022718.
[45] L. Janosi, M. Ceccarelli, The gating mechanism of the human aquaporin 5 revealed by molecular dynamics simulations, PLoS ONE 8 (2013) e59897, http://dx.doi.org/10.1371/journal.pone.0059897.
[46] F. Zhu, E. Tajkhorshid, K. Schulten, Collective diffusion model for water permeation through microscopic channels, Phys. Rev. Lett. 93 (2004) 224501.
[47] M. Hashido, A. Kidera, M. Ikeguchi, Water transport in aquaporins: osmotic permeability matrix analysis of molecular dynamics simulations, Biophys. J. 93 (2007) 373–385, http://dx.doi.org/10.1529/biophysj.106.101170.
[48] J.S. Jung, R.V. Bhat, G.M. Preston, W.B. Guggino, J.M. Baraban, et al., Molecular characterization of an aquaporin cDNA from brain: candidate osmoreceptor and regulator of water balance, Proc. Natl. Acad. Sci. U. S. A. 91 (1994) 13052–13056.
[49] J.S. Hub, C. Aponte-Santamaria, H. Grubmuller, B.L. de Groot, Voltage-regulated water flux through aquaporin channels in silico, Biophys. J. 99 (2010) L97–L99, http://dx.doi.org/10.1016/j.bpj.2010.11.003.
[50] L. Sasseville, J.E. Cuervo, J.Y. Lapointe, S.Y. Noskov, The structural pathway for water permeation through sodium-glucose cotransporters, Biophys. J. 101 (2011) 1887, http://dx.doi.org/10.1016/j.bpj.2011.09.019.
[51] K. Alleva, C.M. Niemietz, M. Sutka, C. Maurel, M. Parisi, S.D. Tyerman, G. Amodeo, Plasma membrane of Beta vulgaris storage root shows high water channel activity regulated by cytoplasmic pH and a dual range of calcium concentrations, J. Exp. Bot. 57 (2006) 609–621, http://dx.doi.org/10.1093/jxb/erj046.
[52] L. Leitão, C. Prista, T.F. Moura, M.C. Loureiro-Dias, G. Soveral, Grapevine aquaporins: gating of a tonoplast intrinsic protein (TIP2;1) by cytosolic pH, PLoS ONE 7 (2012) e33219, http://dx.doi.org/10.1371/journal.pone.0033219.
[53] Y. Yukutake, Y. Hirano, M. Suematsu, M. Yasui, Rapid and reversible inhibition of aquaporin-4 by zinc, Biochemistry (Mosc) 48 (2009) 12059–12061, http://dx.doi.org/10.1021/bi901762y.
[54] Y. Yukutake, M. Yasui, Regulation of water permeability through aquaporin-4, Neuroscience 168 (2010) 885–891, http://dx.doi.org/10.1016/j.neuroscience.2009.10.029.
[55] L. Hedstrom, Serine protease mechanism and specificity, Chem. Rev. 102 (2002) 4501–4523, http://dx.doi.org/10.1021/cr000033x.
[56] R. Sachdeva, B. Singh, Insights into structural mechanisms of gating induced regulation of aquaporins, Prog. Biophys. Mol. Biol. (2014), http://dx.doi.org/10.1016/j.pbiomolbio.2014.01.002.
[57] Schrödinger Release 2013-2, Maestro, version 9.5, Schrödinger, LLC, New York, NY, 2013.
[58] W. Humphrey, A. Dalke, K. Schulten, VMD: visual molecular dynamics, J. Mol. Graph. 14 (33–38) (1996) 27–28.
[59] W.L. Jorgensen, J. Chandrasekhar, J.D. Madura, R.W. Impey, M.L. Klein, Comparison of simple potential functions for simulating liquid water, J. Chem. Phys. 79 (1983) 926–935, http://dx.doi.org/10.1063/1.445869.
[60] J.C. Phillips, R. Braun, W. Wang, J. Gumbart, E. Tajkhorshid, et al., Scalable molecular dynamics with NAMD, J. Comput. Chem. 26 (2005) 1781–1802, http://dx.doi.org/10.1002/jcc.20289.
[61] A.D. MacKerell Jr., N. Banavali, N. Foloppe, Development and current status of the CHARMM force field for nucleic acids, Biopolymers 56 (2000) 257–265, http://dx.doi.org/10.1002/1097-0282(2000)56:4<257::AID-BIP10029>3.0.CO;2-W.
[62] T. Darden, D. York, L. Pedersen, Particle mesh Ewald: an N −log(N) method for Ewald sums in large systems, J. Chem. Phys. 98 (1993) 10089, http://dx.doi.org/10.1063/1.464397.
[63] G.J. Martyna, D.J. Tobias, M.L. Klein, Constant pressure molecular dynamics algorithms, J. Chem. Phys. 101 (1994) 4177–4189, http://dx.doi.org/10.1063/1.467468.
[64] S.E. Feller, Y. Zhang, R.W. Pastor, B.R. Brooks, Constant pressure molecular dynamics simulation: the Langevin piston method, J. Chem. Phys. 103 (1995) 4613–4621, http://dx.doi.org/10.1063/1.470648.
[65] S.A. Adelman, J.D. Doll, Generalized Langevin equation approach for atom/solid-surface scattering: general formulation for classical scattering off harmonic solids, J. Chem. Phys. 64 (2008) 2375–2388, http://dx.doi.org/10.1063/1.432526.
[66] O.S. Smart, J.M. Goodfellow, B.A. Wallace, The pore dimensions of gramicidin A, Biophys. J. 65 (1993) 2455–2460, http://dx.doi.org/10.1016/S0006-3495(93)81293-1.